Department of Veterans Affairs

Journal of Rehabilitation Research and Development
Vol. 39 No. 6, November/December 2002
Pages 635–650

Shoulder kinematics and kinetics during two speeds of wheelchair propulsion

Alicia M. Koontz, PhD, ATP; Rory A. Cooper, PhD; Michael L. Boninger, MD; Aaron L. Souza, MS; Brian T. Fay, PhD

Department of Rehabilitation Science and Technology and Department of Bioengineering, University of Pittsburgh, PA; Department of Physical Medicine and Rehabilitation, University of Pittsburgh Medical Center Health System, Pittsburgh, PA; Human Engineering Research Laboratories, Department of Veterans Affairs Pittsburgh Healthcare System, Pittsburgh, PA

Abstract— The primary objective of this study was to examine the kinematics and kinetics of the shoulder during wheelchair propulsion at a slow and moderate speed. Twenty-seven individuals with paraplegia propelled their wheelchairs at speeds of 0.9 m/s and 1.8 m/s while a motion analysis system captured movements of their upper limbs and SMART^{Wheel}s simultaneously recorded their pushrim kinetics. Intraclass *R* correlation and Cronbach's coefficient alpha statistics revealed that all shoulder parameters were stable and consistent between strokes and speeds. The shoulder exhibited a greater range of motion, and forces and moments at the shoulder were 1.2 to 2.0 times greater ($p < 0.05$) during the 1.8 m/s speed trial. Peak posterior forces occurred near the end of the propulsion phase, and at the same time, the shoulder was maximally flexed and minimally abducted ($p > 0.1$). Shoulder positioning and the associated peak shoulder loads during propulsion may be important indicators for identifying manual wheelchair users at risk for developing shoulder pain and injury.

This material was based on work supported by the U.S. Department of Veterans Affairs (Project B689-RA and B2674-CA), Eastern Paralyzed Veterans of America, National Institutes of Health (NIH K08 HD01122-01), and the National Institute on Disability and Rehabilitation Research Training grant (H133P970013-98). Portions of this work were presented at the Rehabilitation Engineering and Assistive Technology Society of North America (RESNA) 2000 Conference, June 28 to July 2, 2000, in Orlando, Florida, and at the American Society of Biomechanics Annual Meeting, July 19–22, 2000, in Chicago, Illinois.

Address all correspondence and requests for reprints to Alicia M. Koontz, PhD; Human Engineering Research Laboratories, Department of Veterans Affairs Pittsburgh Healthcare System, 7180 Highland Drive, 151R-1, Pittsburgh, PA 15206; 412-365-4833; fax: 412-365-4850; email: akoontz@pitt.edu.

Key words: *biomechanics, kinematics, kinetics, shoulder injury, shoulder pain, spinal cord injury, wheelchair propulsion.*

INTRODUCTION

Wheelchair propulsion has been implicated as a causative factor in developing shoulder pain and injury. An estimated 30 to 75 percent of manual wheelchair users will develop shoulder pain during their lifetime [1–6]. In one study, 72 percent of individuals with a spinal cord injury (SCI) had radiological evidence of degenerative shoulder changes and, in most cases, were asymptomatic [6]. The factors that predispose an individual to developing chronic shoulder pain and pathology are not well understood. These factors may be related to shoulder positioning and repetitive loading occurring at the joint during propulsion.

Several researchers have recorded shoulder movement patterns during propulsion for various groups of wheelchair users. Many of the earlier studies presented a two-dimensional (2D) analysis of shoulder kinematics [7–9], whereas more recently, three-dimensional (3D) analyses have been performed with axial rotation as a third articulation of the humerus [10–13]. These studies have documented that during the propulsion phase of the cycle, the shoulder exhibits internal rotation, abduction, and flexion and extension. In addition, movement patterns vary depending on wheelchair type, level of injury, and speed [11–14].

Only a few investigators have obtained estimates of the net shoulder-joint forces and moments during wheelchair propulsion [8,15–17]. Shoulder kinetics have been determined for propulsion at various speeds, over simulated inclines, and for varying external power outputs [16,17]. Most of the studies on shoulder kinetics have been limited to 2D analyses or static data collection procedures. Limited data regarding 3D shoulder kinetics and kinematics during wheelchair propulsion are available. Peak shoulder forces and moments that occur at or near the end ranges of the shoulder motion may help explain the high prevalence of shoulder pain and pathology among wheelchair users. Therefore, the primary objective of this study was to provide a 3D description of both shoulder kinetics and range of motion during wheelchair propulsion. We hypothesized that—

1. Output parameters of a 3D dynamic shoulder model would produce stable and reliable parameters that describe shoulder biomechanics during propulsion.
2. Shoulder angles, forces, and moments would be statistically different between speeds of propulsion.
3. Maximum and minimum shoulder angles would occur near the same time during the propulsion phase as the peak shoulder forces and moments.

The shoulder girdle is the primary source of power in most activities performed by wheelchair users but, consequently, is more prone to overuse injuries and chronic pain. Determining the overall shoulder stresses and positioning during propulsion may help identify harmful aspects to a manual wheelchair user's stroke, which may be linked to the development of pain and injury. In addition, information about the applied loads to the shoulders during propulsion may be used for the optimization of wheelchair setup and performance and the user may be trained in more effective wheelchair techniques to avoid injuries in the future.

METHODS

This study took place at the Department of Veterans Affairs (VA) Medical Center in Pittsburgh, Pennsylvania, and was approved by the local VA Research and Development Committee, VA Human Studies Subcommittee, as well as the University of Pittsburgh's Institutional Review Board.

Study Participants

The inclusion criteria were (1) complete or incomplete SCI below T1, (2) the use of a manual wheelchair as a primary mode of mobility, (3) the use of a manual wheelchair for at least 1 year, and (4) ages between 18 and 65 years. In addition, brief medical histories were collected from each subject before performing the propulsion trials. This information was used to ensure that subjects did not have a heart condition that could possibly be exacerbated by propelling a wheelchair. Twenty-seven individuals were recruited from within the VA Pittsburgh Healthcare System and from local rehabilitation hospitals and clinics. All subjects provided written informed consent before their participation in this study. The sample consisted of 10 women and 17 men. Their mean ages and years postinjury were 36 ± 10 (range = 20 to 65 years) and 11 ± 5 (range = 1 to 23 years), respectively. The average mass of the subjects was 74.6 kg ± 17.3 kg (range = 43.1 kg to 105.2 kg).

Kinetic Measurement System

Propulsion kinetics were obtained with a SMART-^{Wheel}, which is a 3D force and torque-sensing push rim [18]. Details concerning the system components, percent linearity, and precision of this device have been previously documented [18,19]. Kinetic data from two SMART^{Wheel}s were collected at 240 Hz and filtered with an 8th order Butterworth low-pass filter, zero lag, and a 20 Hz cutoff frequency. The kinetic data were linearly interpolated for synchronization with the kinematic data collection rate of 60 Hz.

Kinematic Measurement System

An OPTO*TRAK* 3020 3D motion analysis system (Northern Digital, Inc., Waterloo, Ontario, Canada) was used to collect position data of infrared-emitting diode markers placed on the wheelchair user's body. The markers were attached with double-sided sticky tabs to the bony landmarks on the arm (**Figure 1**): most lateral part of the acromion process, lateral epicondyle, olecranon, third and fifth metacarpalphalangeal joints (not shown), and radial and ulnar styloids.

This system was configured to collect the real-time movement patterns of the entire arm, head, and torso during propulsion. Two cameras were positioned, facing each other, on either side of the subjects to capture movement patterns bilaterally. A synchronization pulse from the OPTO*TRAK* was used to trigger the start of kinetic and kinematic data collection. Kinematic data were collected at a 60 Hz sampling frequency and filtered with a 4th order Butterworth low-pass filter, zero lag, and a 7 Hz cutoff frequency.

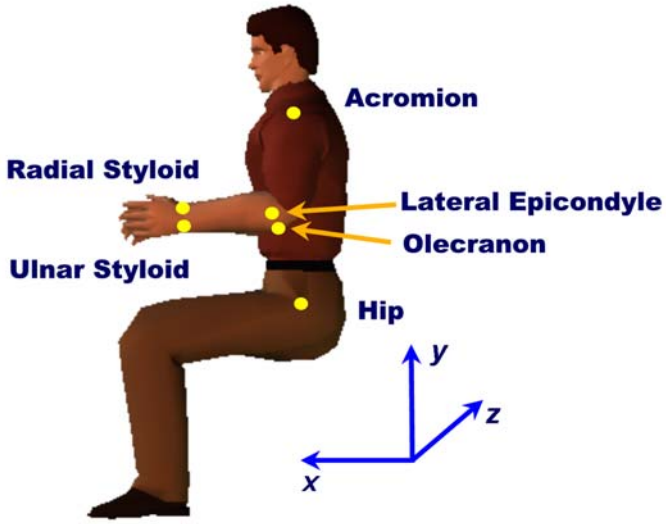

Figure 1.
Marker placement and global coordinate system axis representation.

Data Collection

Subjects used their personal wheelchairs in this study, and their wheelchairs were not altered, with the exception of replacing their original rear wheels with the SMART-^{Wheel}s. All subjects used a standard smooth push rim of 0.88 cm in tube diameter and 52.7 cm overall rim diameter.

Wheelchairs were centered between the two motion analysis cameras and secured to a dynamometer, with a resistance comparable to that of a smooth level tile surface [20]. Subjects were provided with an acclimation period for at least 5 minutes before data collection to become accustomed to propelling on the dynamometer. Afterward, participants were instructed to propel at two constant speeds of 0.9 m/s (2 mi/h) and 1.8 m/s (4 mi/h). They monitored their own speed using a video computer monitor that displayed the forward velocity and the differential velocity of the roller system. Subjects propelled at the target speeds for at least 1 minute before 20 s of kinetic and kinematic data were collected.

Data Analysis

Biomechanical Shoulder Model

We determined shoulder joint angles and forces using a local coordinate system (LCS) approach described by Cooper and colleagues [21]. The analysis was limited to movements and kinetics of the glenohumeral joint because of the difficulties in measuring the positions of the scapula, clavicle, and thoracic spine movement during propulsion. Shoulder motion was described relative to the trunk. In this analysis, the trunk was restricted to moving in the sagittal plane only. A recent finding of Cooper et al., who investigated various shoulder and trunk representations, concluded that only allowing the trunk to flex produced similar results as if the trunk were allowed to freely rotate [21]. Limb segments were assumed to be rigid with uniform density. Body weight, segment lengths, and circumferences were obtained from each wheelchair user in the study. Segment mass, segment center of mass, and inertias of the hand, forearm, and upper arm were computed according to the methods described by Hanavan and Clauser et al. and entered into the model [22,23]. The output variables of the biomechanical model were the time-varying 3D net joint muscle forces acting at the glenohumeral joint (along a anterior/posterior axis (x), superior/inferior axis (y), and medial/lateral axis (z), shoulder angles expressed in anatomical terms, and the net moments acting to flex/extend (z), abduct/adduct (x), and internally/externally rotate the arm (y')). The "right-hand rule" was used to define positive forces and moments. Sagittal flexion, horizontal flexion, abduction, and internal rotation angles were positive. All angles were determined in reference to a neutral anatomic position, that is, with the arm straight down to the side, palm facing in toward the body. All equations and postprocessing analyses were implemented in MATLAB (Mathworks, Inc., Natick, Massachusetts).

Data Reduction

Shoulder joint angles, forces, and moments were analyzed for five propulsion strokes across each speed trial. The stroke has generally been divided into two phases: a drive or propulsion phase and a recovery phase [24,25]. The onset of propulsion was defined as the point at which the propulsive moment at the push rim, as measured by the SMART^{Wheel}s, deviated from the baseline by 5 percent. The end of propulsion and the beginning of recovery were defined as the point at which the propulsive moment at the push rim returned to baseline and remained within 5 percent. From the motion, force, and moment curves, peak values during the propulsion phase were obtained. Each stroke was analyzed separately. The time instance at which the maximum and minimum angles, forces, and moments occurred was expressed as a percentage of the propulsion phase, since time spent in this phase varied across individuals and across strokes.

Statistical Analysis

We used a two-step approach to determine if the shoulder model produced consistent and reliable parameters across multiple strokes and speeds. First, the interstroke reliability was evaluated by intraclass *R* correlation coefficients (ICC). The ICCs were computed separately for each model parameter, each speed, and each side. A parameter was considered reliable if intraclass *R* was > 0.60 at both speeds [26]. Second, for parameters that met the preceding criterion, we computed Cronbach's alpha coefficient to determine the increased reliability of creating aggregated scores across the repeated strokes. The summed score was considered to have good reliability if the alpha coefficient was > 0.80 at both speeds and sides [27]. For parameters that met both of these conditions, the peak forces, moments, and maximum and minimum angles were averaged across strokes for each side. We then performed Pearson product-moment correlations to assess the strength of the right and left side associations among the shoulder variables. Since the sides were correlated ($p < 0.05$, minimum $r > 0.6$), peak shoulder values were averaged across sides for each speed trial. Paired t-tests were conducted to test for significant performance differences between the two speed trials. A p value less than 0.05 was considered statistically significant. Paired t-tests were also used to test for similarities between the relative timing of the peak shoulder force and moment variables and the maximum and minimum angles ($p > 0.10$). Experiment-wise error rate control procedures were not used. All statistics were performed in the SPSS statistical package (SPSS, Inc., Chicago, Illinois).

RESULTS

Descriptive

All model output parameters met the criteria for reliability and stability; therefore, all the parameters underwent further analysis. **Table 1** lists propulsion characteristics for the group. Participants had no difficulty maintaining the 0.9 m/s target speed, but some had trouble reaching and/or maintaining the fast speed of 1.8 m/s. The average number of strokes per second was greater, while total cycle time and the amount of time spent in contact with the push rim were shorter during the 1.8 m/s speed condition. The angle of hand contact relative to the horizontal (+*x*-axis) and the overall contact angle on the push rim during the propulsion phase are also shown in **Table 1**. Subjects propelled with smaller hand push rim contact angles at the fast speed (100.3° and 110.3°, respectively).

Shoulder Motion During Propulsion

Each figure in the paper (except **Figures 2** and **3**) represents a different subject. Figures containing data for five strokes demonstrate the stroke-to-stroke variability within a subject. **Table 2** contains the group mean maximum and minimum shoulder angles and relative timing during the propulsion phase for both speed conditions. Also, shoulder angles for five stroke cycles at the slowest speed are presented for a single subject in **Figure 4**.

As illustrated in **Figure 4**, the shoulder started in a position of extension and progressed to flexion in both the sagittal and horizontal plane views. The arms remained abducted throughout the entire cycle and reached an average peak 29 percent into the propulsion phase (**Table 2**). For most subjects, a second peak was observed later during the recovery phase and just before hand contact. Only three of the subjects externally rotated their shoulders during the 1.8 m/s speed trial, and therefore, only internal rotation angles were reported for the group. A general pattern of decreasing internal rotation during the propulsion phase and increasing rotation during the recovery phase was observed. Shoulders were minimally abducted and internally rotated near the end of the propulsion phase. For both speeds tested, the overall ranges of shoulder motion were larger for sagittal flexion/extension (62.3° and 68.6°) and horizontal flexion/extension (84.6° and 93.6°).

Table 1.
Group propulsion characteristics for both speed conditions: 0.9 m/s and 1.8 m/s. Group means and standard deviations are in parentheses. Push time is time during which hand was in contact with push rim. Start and contact angles are reported relative to horizontal axis.

Speed (m/s)	Actual Speed (m/s)	Cadence (stroke/s)	Total Cycle (s)	Push Time (s)	Start Angle (°)	Contact Angle (°)
0.9	0.97 (0.12)	0.97 (0.20)	1.06 (0.19)	0.52 (0.09)	119.55 (11.4)	100.3 (16.6)
1.8	1.61 (0.23)	1.32 (0.22)	0.77 (0.12)	0.35 (0.05)	119.03 (10.5)	110.3 (15.8)

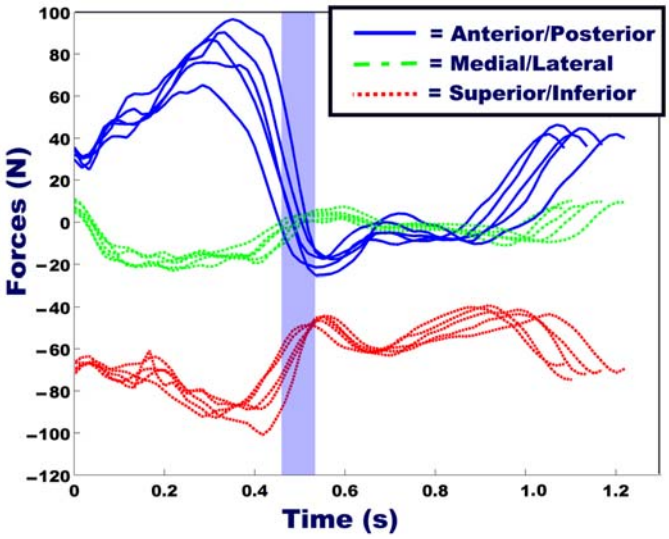

Figure 2.
Shoulder forces versus time during propulsion at 0.9 m/s: Five consecutive strokes for a single subject are represented. Beginning of stroke is at time = 0 s. Anterior, medial, and superior force components were positive. Blue area represents transition between propulsion phase and recovery phase.

Shoulder Kinetics During Propulsion

Table 3 and **Table 4** display the group's mean peak 3D net shoulder forces and moments and the relative timing of the peaks for both speed conditions.

Forces

At both speeds, the greatest forces were present during the propulsion phase with the highest magnitudes in the inferior direction (90.0 N, 108.2 N), followed by the anterior (59.9 N, 86.6 N), and then the medial directions (34.0 N, 50.4 N). As the stroke progressed, the magnitudes of the anterior, inferior, and medial force components continued to increase until they reached their peaks for each speed at 44.5 percent and 38.5, 63.6 and 55.5 percent, and 57.9 and 56.4 percent of the propulsion phase, respectively. After this point, the anterior force rapidly decreased and changed directions at the end of the propulsion phase and the beginning of recovery. Inferior forces generally decreased and leveled off at a constant value equal to the weight of the limb. Forces in the anterior/posterior and medial/lateral directions diverged to values close to zero. Only four subjects displayed forces directed in the superior direction during the 1.8 m/s speed trial. The magnitude of this force was small (<8 N), and therefore, only inferior forces were reported for the group in **Table 3**. The shoulder joint force components for a single subject during the slowest speed trial are depicted in **Figure 2**.

Moments

At both speeds tested, the moment responsible for flexing the arm in the sagittal plane was the largest (28.6 N•m,

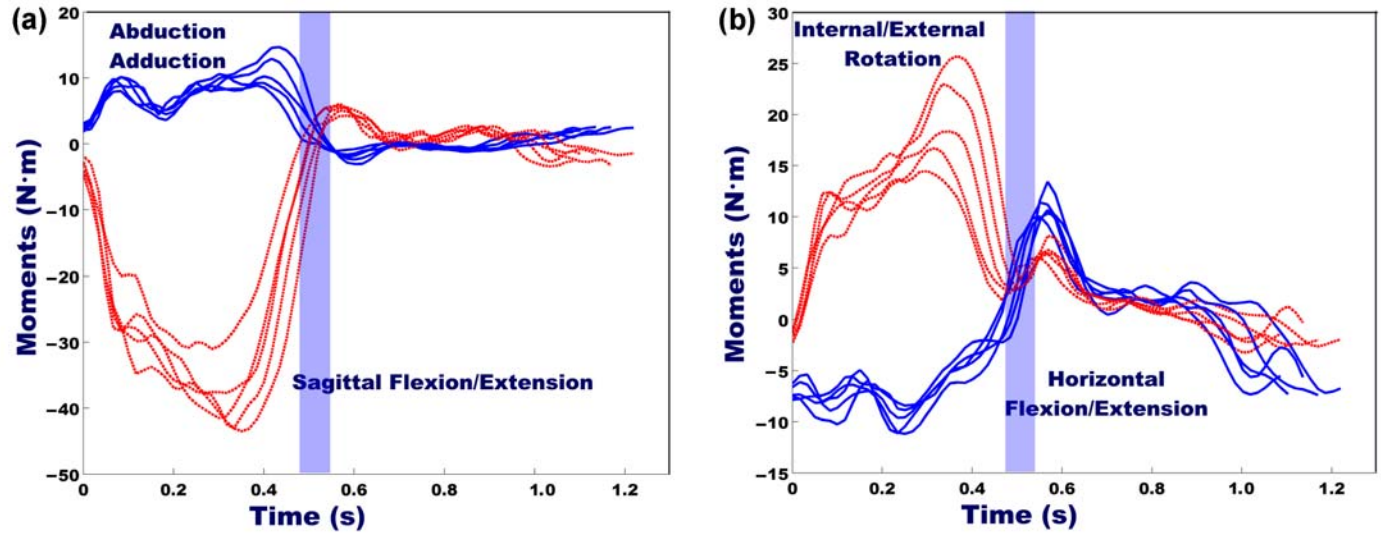

Figure 3.
Shoulder moments during propulsion at 0.9 m/s: Five consecutive strokes for a single subject are presented. Beginning of stroke is at time = 0 s. **(a)** Abduction/adduction moment (top) and sagittal flexion/extension moment (bottom) and **(b)** shoulder internal rotation angle (top) and horizontal flexion/extension angle (bottom). Adduction, sagittal extension, internal rotation, and horizontal flexion moments are positive. Blue area represents transition between propulsion phase and recovery phase.

Table 2.
Maximum and minimum shoulder angles and relative timing during propulsion phase of stroke (% push) at 0.9 m/s and 1.8 m/s. Shoulder angles are maximums unless otherwise noted. Group means and standard deviations are in parentheses.

Shoulder Angle	Angle (°)		*p* Value	% Push		*p* Value
	0.9 m/s	1.8 m/s		0.9 m/s	1.8 m/s	
Sagittal Flexion	19.1 (6.6)	23.2 (8.3)	0.000	99.7 (0.8)	97.5 (5.1)	0.028
Sagittal Extension	43.2 (5.7)	45.4 (5.1)	0.001	7.8 (6.2)	7.7 (4.1)	0.406
Abduction	42.0 (6.7)	42.0 (6.5)	0.937	29.1 (18.3)	28.7 (18.8)	0.828
Minimum Abduction	26.0 (4.1)	25.0 (4.1)	0.006	96.0 (10.8)	94.3 (14.1)	0.513
Internal Rotation	52.1 (11.3)	51.4 (12.2)	0.509	15.1 (22.1)	24.5 (23.0)	0.686
Minimum Internal Rotation	24.5 (11.0)	22.8 (10.5)	0.101	88.7 (9.8)	84.8 (13.0)	0.832
Horizontal Flexion	34.4 (9.3)	41.2 (10.2)	0.000	99.8 (0.6)	97.7 (4.8)	0.037
Horizontal Extension	50.2 (7.4)	52.4 (7.4)	0.001	9.2 (5.3)	9.3 (4.5)	0.787

36.5 N•m), followed by the internal rotation moment (21.6 N•m, 31.9 N•m), adduction moment (21.3 N•m, 31.1 N•m), and horizontal flexion moment (10.9 N•m, 21.0 N•m). These moments were generally small at the beginning of propulsion and then reached their peaks midway into the propulsion phase, except the peak horizontal flexion moment, which occurred closer to the end (87.5%, 92.2%). The moments acting to extend, externally rotate, and abduct the shoulder were much smaller (<6.7 N•m). Peak sagittal extension and peak abduction occurred at the end of the propulsion phase (90.9%, 87.8%, and 86.7%, 92.8%, respectively). Peak horizontal extension moment and external rotation moment occurred 29.4 and 27.9 percent into the propulsion phase during the slowest speed and 30.7 and 24.3 percent into the propulsion phase during the fast speed. All moments leveled off to a point close to zero shortly into the recovery phase. Moments at the shoulder for a single subject propelling at 0.9 m/s are illustrated in **Figure 3**.

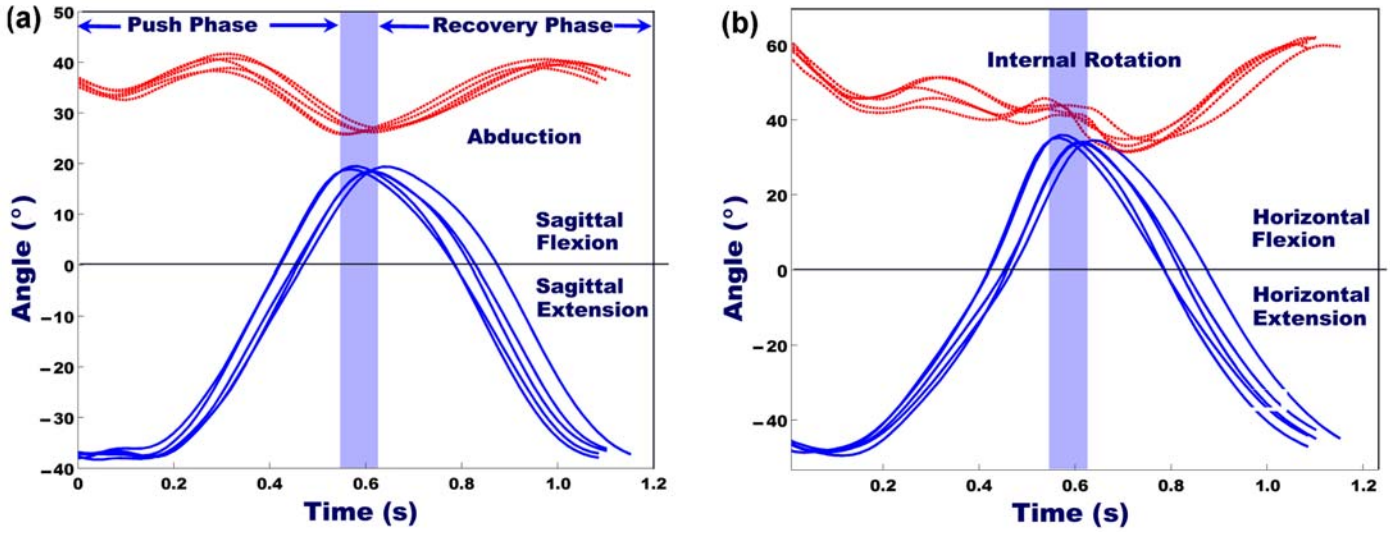

Figure 4.
Shoulder movement versus time during propulsion at 0.9 m/s: Five consecutive strokes for a single subject are represented. Beginning of stroke is at time = 0 s. **(a)** Abduction angle (top) and sagittal flexion/extension angle (bottom) and **(b)** shoulder internal rotation angle (top) and horizontal flexion/extension angle (bottom). Blue area represents transition between propulsion phase and recovery phase. This could not be represented as a single line, since transition time varied slightly between strokes.

Table 3.
Peak shoulder forces and relative timing during propulsion phase (% push) at 0.9 m/s and 1.8 m/s. Group means and standard deviations are in parentheses. Cosθ, cosθy, and cosθz are direction cosines of resultant force (FR) at shoulder relative to horizontal, vertical, and transverse axes, respectively.

Shoulder Forces (N)	Peak		*p* Value	% Push		*p* Value
	0.9 m/s	1.8 m/s		0.9 m/s	1.8 m/s	
Anterior	59.9 (18.4)	86.6 (29.0)	0.000	44.5 (10.9)	38.5 (9.6)	0.028
Posterior	17.1 (9.9)	36.8 (12.2)	0.000	97.2 (7.4)	95.8 (6.2)	0.124
Inferior	90.0 (36.2)	108.2 (45.1)	0.000	63.6 (8.1)	55.5 (9.2)	0.001
Medial	34.0 (21.5)	50.4 (28.5)	0.000	57.9 (11.6)	56.4 (12.5)	0.692
Lateral	7.1 (5.3)	14.9 (7.4)	0.000	59.0 (27.8)	72.5 (29.3)	0.025
FR	112.8 (37.7)	145.3 (46.3)	0.000	60.4 (7.9)	50.2 (8.5)	0.000
Average FR	79.4 (25.8)	82.9 (24.9)	0.002	—	—	—
Direction Cosines FR (°)						
Cosθx	59.8 (7.2)	55.9 (8.0)	0.000	—	—	—
Cosθy	141.9 (10.8)	136.0 (12.7)	0.000	—	—	—
Cosθz	72.8 (11.8)	71.6 (15.0)	0.469	—	—	—

Table 4.
Peak shoulder moments and relative timing during propulsion phase (% push) at 0.9 m/s and 1.8 m/s. Group means and standard deviations are in parentheses.

Shoulder Moments (N•m)	Peak		*p* Value	% Push		*p* Value
	0.9 m/s	1.8 m/s		0.9 m/s	1.8 m/s	
Sagittal Flexion	28.6 (8.6)	36.5 (11.5)	0.000	46.5 (8.6)	46.7 (12.7)	0.360
Sagittal Extension	3.9 (2.6)	7.1 (3.6)	0.000	90.9 (12.1)	87.8 (16.4)	0.962
Abduction	2.2 (2.5)	5.1 (4.3)	0.000	86.7 (19.3)	92.8 (11.2)	0.552
Adduction	21.3 (12.0)	31.1 (14.1)	0.000	63.4 (12.3)	58.1 (13.4)	0.025
Internal Rotation	21.6 (5.9)	31.9 (10.7)	0.000	48.4 (10.3)	51.1 (16.8)	0.342
External Rotation	2.3 (1.5)	4.6 (3.4)	0.000	30.7 (27.9)	24.3 (21.2)	0.188
Horizontal Flexion	10.9 (6.3)	21.0 (10.2)	0.000	87.5 (18.3)	92.2 (10.9)	0.228
Horizontal Extension	6.7 (3.5)	10.5 (5.7)	0.000	29.4 (19.2)	27.9 (22.2)	0.703

Speed Differences

Shoulder Movement

Sagittal flexion, sagittal extension, minimum abduction, horizontal flexion, and horizontal extension angles were significantly different between speeds ($p < 0.05$). The overall range of flexion/extension motion was greater for the fast speed (62.3°, 68.6°), and a more rapid increase to achieve peak flexion was present (99.7%, 97.5%). During the recovery phase, the shoulder moved from flexion to extension at a similar rate at both speeds. In both speed trials, the maximum internal rotation angle occurred at the beginning of the propulsion phase (15.1%, 24.5%). The minimum internal rotation angle occurred near the end and slightly earlier during the fast speed trial (88.7%, 84.8%). During the recovery phase, arm rotation increased at both speeds at approximately the same rate. The overall degree of internal rotation exhibited during each speed condition was consistent across speeds (39.8°, 40.4°).

Shoulder Forces

All peak shoulder forces were significantly larger ($p < 0.002$) for the fast speed condition (**Table 3**). The mean

anterior force increased by 26.7 N, inferior force increased by 18.2 N, and medial force increased by 16.4 N. Posterior and lateral force components increased twofold (23.7 N and 7.8 N, respectively). All peak shoulder forces occurred earlier during the fast speed trials with the exception of the lateral force component. However, only the relative timing of the peak anterior (44.5%, 38.5%), inferior (63.6%, 55.5%), and lateral (59.0%, 72.5%) shoulder force components and the resultant force at the shoulders (60.4%, 50.2%) were significantly different between speeds.

Shoulder Moments

All peak shoulder moments were significantly larger for the fast speed trial (**Table 4**). Internal rotation moment was greater during the fast speed trial by 10.3 N•m, horizontal flexion moment by 10.1 N•m, adduction moment by 9.8 N•m, sagittal flexion moment by 7.9 N•m, and horizontal extension moment by 3.8 N•m. The other peak moments were nearly twice as large (sagittal extension (3.9 N•m, 7.1 N•m), abduction (2.2 N•m, 5.1 N•m, and external rotation (2.3 N•m, 4.6 N•m). Contrary to the shoulder forces, shoulder moments acting to flex and internally rotate the shoulder peaked later, although not significantly, at the fast speed. The adduction moment peaked 5.3 percent sooner during the fast speed trial. Moments responsible for extending and externally rotating the arm peaked earlier at the fast speeds.

Force/Moment Versus Angle Relationship

Table 5 lists the results of the paired t-test statistics used to compare the relative timing of the peak kinetic variables and the minimum and maximum angles. Interestingly, the relative timing of the peak shoulder forces and moments components coincided more frequently with the timing of the maximum and minimum angles at the fast speed. The pairs that were significant at the slow speed were also significant at the fast speed except for pairings between the minimum internal rotation angle and the abduction moment and horizontal flexion moment.

Figure 5 illustrates the relationship between the anterior/posterior force and the sagittal flexion/extension angle at 1.8 m/s for a single subject and stroke. The peak posterior force occurred approximately the same time as the peak sagittal flexion angle. Although this subject's anterior force peaked nearly 40 percent into the propulsion phase, the position of the shoulder was also near maximum extension. Sagittal extension moment peaked when the shoulder was minimally abducted (**Figure 6**).

Table 5.
Results of comparisons between relative timing of peak shoulder kinetics and minimum and maximum angles during propulsion phase at 0.9 m/s and 1.8 m/s. All angles listed are maximums unless otherwise noted. Corresponding *p* values for only those pairings that were statistically similar are listed. Average group mean differences for each pairing are also provided.

Kinetics	Angle	0.9 m/s *p* Value	Difference (%)	1.8 m/s *p* Value	Difference (%)
Posterior Force	Sagittal flexion	—	2.5	0.18	1.7
	Minimum abduction	0.65	1.2	0.61	1.5
	Horizontal flexion	—	2.6	0.11	1.9
Moments					
Sagittal Extension	Minimum abduction	0.11	5.1	0.13	6.5
	Minimum internal rotation	0.49	2.2	0.49	3.0
Abduction	Minimum abduction	—	9.3	0.66	1.5
	Minimum internal rotation	0.67	2.0	—	8.0
Horizontal Flexion	Minimum abduction	—	8.5	0.43	2.1
	Minimum internal rotation	0.78	1.2	—	7.4
Horizontal Extension	Abduction	0.95	0.4	0.90	0.8
	Internal rotation	—	14.3	0.62	3.4
External Rotation	Abduction	0.82	1.6	0.40	4.4
	Internal rotation	—	15.6	0.98	0.2

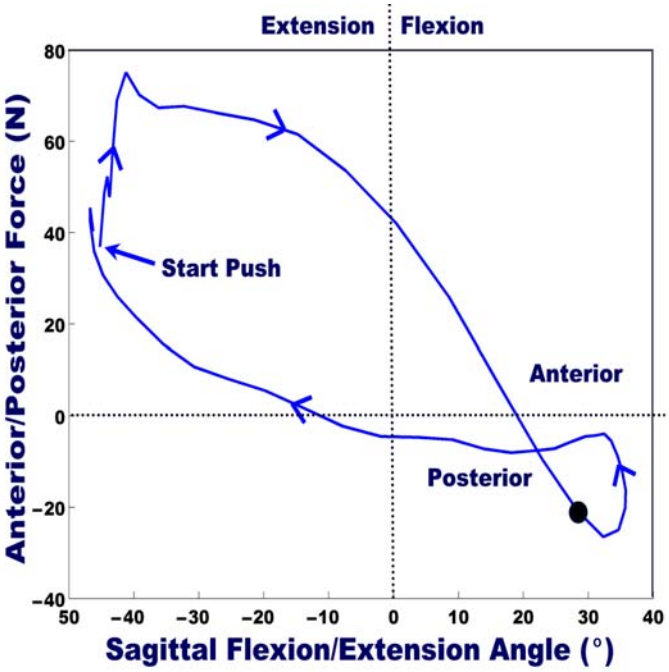

Figure 5.
Shoulder anterior/posterior force versus sagittal flexion/extension angle: A single stroke from a single subject pushing at 1.8 m/s is shown. Anterior force and sagittal flexion angle were positive. Beginning of stroke is near left side of plot and progresses to right. Dark circle represents transition between propulsion phase and recovery phase.

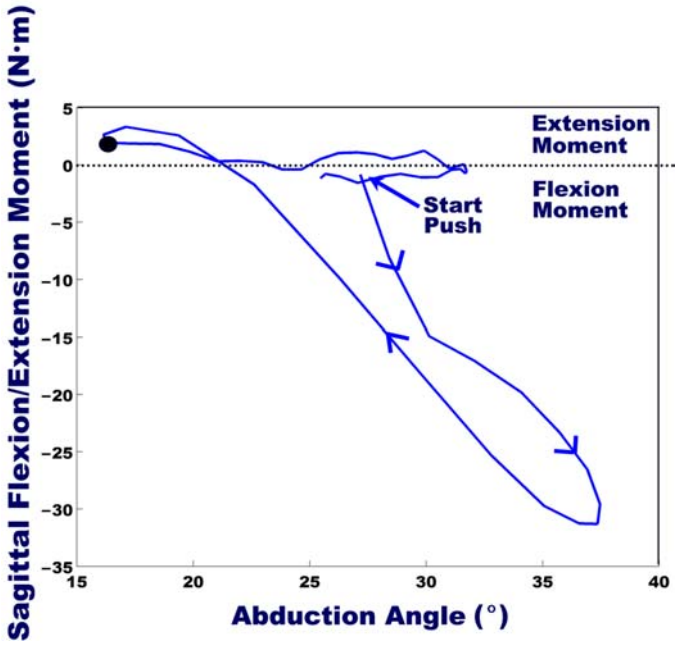

Figure 6.
Shoulder sagittal flexion/extension moment versus abduction angle: A single stroke from a single subject pushing at 1.8 m/s is shown. Sagittal extension moment was positive. Beginning of stroke is near upper center of plot and progresses downward and then left. Dark circle represents transition between propulsion phase and recovery phase.

In addition, the sagittal flexion moment peaked midway into the propulsion phase when the shoulder was maximally abducted.

DISCUSSION

This study was conducted to evaluate the reliability and stability of a 3D shoulder inverse-dynamic model and gain insight into the loads acting at the shoulders during wheelchair propulsion at a slow and fast speed. We also studied movement patterns of the shoulders to investigate if high loads occurred at the same time the shoulder was at or near its end ranges of motion. The model used in this study was adopted from Cooper et al. and provided the anatomical shoulder angles and 3D forces and moments at the shoulder [21]. We found that the model produced motion, force, and moment patterns that were consistent, similar, and repeatable across strokes and speeds.

Shoulder Motion

The abduction angles observed in this study compare favorably with those reported by Rao et al., Davis and Growny, Boninger et al., and Newsam et al. whose studies all focused on describing 3D upper-limb kinematics during wheelchair propulsion (**Table 6**) [10–12,14]. Notable differences were found between the studies in shoulder flexion/extension and internal rotation. These differences are likely related to the data collection procedures (e.g., marker set and placement and tracking capabilities), experimental setup (e.g., use of a test wheelchair versus personal wheelchair), and the methods used to calculate the angles.

For instance, the origins of the humeral coordinate systems used to define the motions were located at different positions on the upper arm or glenohumeral joint. This study and the study conducted by Boninger et al. calculated shoulder angles by projecting the vector defining the long axis of the humerus relative to the torso onto the 2D anatomical planes [12]. The internal/external rotation angle resulted from rotating this vector through two angles and then projecting the rotated vector onto the torso coordinate

Table 6.
Comparison between studies of shoulder angles during wheelchair propulsion. Primary authors are listed and test condition (if multiple groups or conditions) was tested.

Study	Sagittal Extension/Flexion (°)	Abduction Max/Min (°)	Internal Rotation Max/Min (°)
Current Study, 0.9 m/s	43.2/19.1	42.0/26.0	52.1/24.5
Rao et al. [10]	57.3/23.2	56.6/22.5	86.2/11.6
Newsam et al. [14] (Low Para Group)	53.6/21.8	56.9/22.1	78.0/24.4
Davis et al. [11] (Quickie 2 Wheelchair)	59.2/27.6	48.2/26.6	57.9/2.1
Boninger et al. [12] (1.3 m/s Speed)	64.0/6.2	47.0/24.5	90.7/55.2

system. Rao et al., Davis and Growny, and Newsam et al. determined all shoulder angles using an Euler angle scheme [10,11,14]. An advantage of the projection angle approach described by Boninger et al. is that the shoulder position in the transverse plane (horizontal flexion/extension angles) can be described [12]. The Euler representation results in only three humeral rotations defining sagittal flexion/extension, abduction/adduction, and internal/external rotation [28], whereas the projection angle approach results in four angles. Although similar methods were used to calculate the shoulder angles, torso orientation was defined and measured differently. Variations in the approaches used to describe trunk movement may have resulted in differences between the studies, particularly in the flexion/extension and internal rotation angles. In all the studies listed in **Table 6**, participants were evaluated in a common test wheelchair, whereas all participants in this study were tested in their own wheelchairs. Studies have shown that shoulder-joint range of motion as well as biomechanical measures of mechanical efficiency and push-rim kinetics is affected by seat and rear axle position [29–32].

Maximum and minimum shoulder angles tended to occur at or near the beginning and end of the push with the exception of the maximum abduction angle, which peaked around 29 percent of the propulsion phase. This was consistent with other studies, except for Rao et al. and Newsam et al. who found maximum abduction angles to occur closer to the beginning of the push [10,14].

Individuals in this study changed their shoulder movement pattern depending on how fast they propelled. As speed increased, subjects executed the propulsion phase faster and spent less time in contact with the push rim. This action would explain why the maximum angles achieved during the propulsion phase occurred sooner during the fast speed trial. The greatest degree of shoulder movement took place in the sagittal and horizontal plane views, and less in rotation and abduction at the faster speed. This finding was consistent with Wang et al.'s study that investigated the 3D upper-limb kinematics of wheelchair racers during four different racing speeds [13].

Boninger and colleagues performed a shoulder kinematic analysis of six Paralympic wheelchair athletes at two speeds slightly faster than those in this study [12]. The overall difference in the horizontal and sagittal flexion/extension range of motion between speeds in Boninger et al.'s study (12.0° and 9.7°) was similar to that observed in this study (9.0° and 6.3°). However, the athletes had greater maximum abduction angles at both speeds and were less abducted at the end of the push than the subjects in this study were. A much larger change between speeds in the abduction range of motion was noted in Boninger et al.'s study. In addition, the athletes overall range of shoulder rotation increased by 6° between speeds compared to 1° for subjects in this study. All the athletes were evaluated in the same test wheelchair, and no adjustments were made to accommodate for body dimension or to emulate their current wheelchair setup. If the wheelchair did not fit the athlete properly (seat was too low or high, seat was too narrow or wide, rear axles were too far forward or rearward), this could have resulted in different shoulder ranges of motion than if the wheelchair was optimally fit to the individual. It is also possible that the differences between the studies are partly because of the subject pool. The data in this study represent nonathletic men and women manual wheelchair users. All the subjects in Boninger et al.'s study were young men who participated in a variety of wheelchair sports, including wheelchair racing. Trained athletes may push differently than nonathletic wheelchair users because they have adopted a propulsion technique that enhances their performance on the track.

Shoulder Net Forces and Moments

The shoulder kinetic data were compared to the work of Kulig and colleagues who presented 3D shoulder kinetic data at two speeds [17]: freely chosen and fast for 17 men with low-level paraplegia. Both speeds were self-selected and average propulsion velocities for the trials were determined afterward. The average "free" and "fast" velocities were 1.5 m/s and 2.3 m/s, respectively. The kinetics described by Kulig et al. were the reaction forces and moments acting at the shoulder joint, whereas the kinetics described in this study were "action" forces and moments [17]. In **Table 7**, Kulig et al.'s reaction force data are listed as anterior (posterior), inferior (superior), and lateral (medial) directions and their moments are sagittal flexion (extension), adduction (abduction), and internal rotation (external rotation) so as to be consistent with the presentation of the kinetic data in this study. Peak forces and moments occurring in the opposite directions (anterior, inferior, medial, sagittal flexion, adduction, and internal rotation) were not reported.

Kulig et al. also found the magnitudes of the anterior and inferior action forces significantly increased between speeds [17]. Compared to this study, anterior forces recorded at the slowest speeds were greater and lower for the fast speeds. The mean magnitudes of the inferior forces presented in Kulig et al. were much lower than those in this study, but their model did not include the mass of the limb [17]. The inferior force component may be the most harmful because it is directed along the longitudinal axis of the arm, forcing the humerus further up into the joint. This increases the demand on the stabilizing muscles of the humeral head (rotators) to oppose this force and keep the humeral head from displacing into the acromiohumeral space and impinging the supraspinatus tendon against the overlying acromioclavicular arch.

Subjects in the Kulig et al.'s study reached their peak magnitudes of anterior force sooner than ours. Inferior forces also occurred sooner at both speeds tested [17]. Kulig et al. did not report the corresponding shoulder kinematics for their subjects. However, we found that the relative timing of the subjects' peak shoulder angles followed a similar trend to the forces as they also occurred earlier during the fast speed trial.

The differences observed between this study and Kulig et al.'s may be attributable partly to variations among the propulsion speeds and the upper-limb models used to describe shoulder joint kinetics. Kulig et al.'s study described shoulder forces and moments in a global frame of reference and not relative to the torso. Trunk range of motion in typical wheelchair propulsion has been shown to vary from subject to subject and can be a high as 15° [33,34]. Thus, neglecting trunk flexion could have confounded the shoulder force calculations.

Also important to note is that the instrumentation used to record the external push-rim forces and moments in Kulig et al.'s shoulder model was limited to the sagittal plane. A theoretical medial-lateral push-rim force was defined by imposing 5° of wheel camber for all subjects and determining the inclined component of the vertical force at the push rim. In this study, a full 7° of freedom push-rim measuring device, SMART^{Wheel}, was used to collect applied 3D push-rim forces and moments for the shoulder model. In our analysis, we accommodated for camber by transforming the 3D push-rim forces and

Table 7.
Peak shoulder forces and moments and relative timing of during propulsion phase (% push) during wheelchair propulsion at two speeds reported in Kulig et al. and current study [17].

Kinetic Variables Forces (N) Moments (N•m)	Current Study 0.9 m/s	Kulig 1.5 m/s	Current Study 1.8 m/s	Kulig 2.3 m/s
Anterior Force/% Push	59.9/44.5	46.3/15.6	86.8/38.5	97.5/28.1
Inferior Force/% Push	90.0/63.6	14.3/53.1	108.2/55.5	75.5/34.4
Lateral Force/% Push	7.1/59.0	7.8/6.3	14.9/72.5	12.9/3.1
Resultant Force/% Push	112.8/54.1	50.9/26.3	145.3/46.3	125.2/33.8
Flexion Moment/% Push	28.6/46.5	13.8/28.1	36.5/46.7	32.5/28.1
Adduction Moment/% Push	21.3/63.4	9.8/15.6	31.1/58.1	20.2/26.6
External Rotation/% Push	2.3/30.7	5.8/12.5	4.6/24.3	13.3/23.4

moments by homogenous transformation matrix about the *x*- and *y*-axes, respectively [35]. The degree of camber varied among individuals from 0° to 6°, since they were tested in their own wheelchairs. Interestingly, the medial reaction forces in both studies were small and compared favorably between this study and that of Kulig et al. [17]. Shoulder lateral reaction forces were not reported in Kulig et al.; however, we found that these forces were at least four times larger than the medial reaction forces at both speeds. This force drives the humeral head into the glenoid cavity and may help stabilize the shoulder joint throughout the push. The inability to record medial-lateral push-rim forces limits the applicability of Kulig et al.'s shoulder model for fully describing 3D net shoulder kinetics during propulsion.

Van der Helm and Veeger in their quasistatic analysis of wheelchair propulsion reported that joint forces depended on hand position and were highest when the hand was at the top dead center (TDC) on the push rim and at 15° in front of the TDC [15]. From the start and stop angles recorded in this study, we estimated that subjects reached the TDC approximately 23 percent into the propulsion phase and were at 15° in front of the TDC at 41 percent into the propulsion phase. Many of the peak forces occurred further in front of this point. This may be a result of the dynamics of wheelchair propulsion because the subjects in van der Helm and Veeger's study were tested under static conditions.

We discovered that the resultant forces at the shoulder were highly correlated to the total forces measured at the push rim (**Figure 7**). A large component of the resultant shoulder forces (approximately 70 percent) is due to the external forces (push-rim forces). The remainder 30 percent is due to joint dynamics and gravitational effects. In a previous study, we found the resultant and radial push-rim forces were significantly correlated with magnetic-imaging evidence of shoulder pathology in wheelchair users [36]. It is possible that stronger relationships between propulsion biomechanics and injury will be discovered when shoulder dynamics are added to the analyses.

Moments acting to flex the humerus in the plane of the wheel were the highest followed by internal rotation, adduction, and horizontal flexion at both speeds. In accordance, Kulig et al. and Veeger et al. found the greatest moment was in flexion for all speed conditions tested [17,37]. Both sagittal flexion and adduction moments reported by Veeger et al. and those reported during the

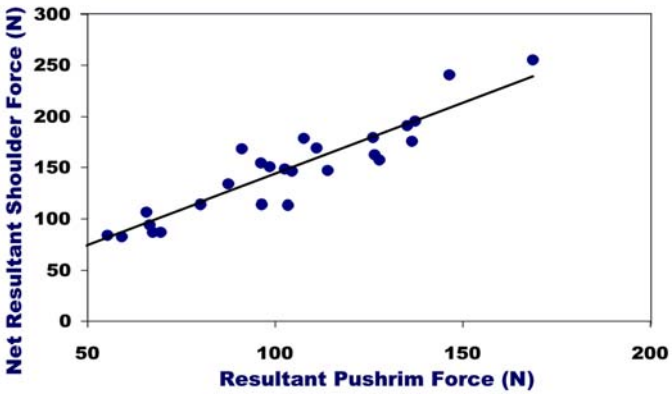

Figure 7.
Relationship between net resultant shoulder force and resultant push-rim force: Pearson correlation r^2 value was 0.86.

"fast" trial in Kulig et al. were closer in agreement to the moments observed in this study [17,37]. All the authors found that directions of the moments tended to reverse near the end of the push phase. Similar to Kulig et al.'s study [17], the moment magnitudes increased significantly between speeds and were on average 1 1/2 times larger for the fast speed.

Moments tended to peak sooner during the fast speed trials, which may explain why the moments in Kulig et al.'s study peaked even earlier, since the average propulsion test speeds were higher [17]. External rotation moment peaked at approximately the same time during the propulsion phase in both studies. Peak horizontal extension moments also occurred around this time. Both the external rotation moment and horizontal extension moments are likely acting to stabilize the shoulder in the initial onset of the stroke while facilitating the much larger flexion moment that generates forward propulsion. None of the other studies reported internal rotation moments, yet we found them to be just as high as the adduction moments. Peak internal rotation moments were over nine times greater than the peak external rotation moments at the slow speed. Adduction moments were almost 10 times greater than the abduction moments, and sagittal flexion moments were seven times larger than the sagittal extension moments. Consequently, a tendency to develop a strength imbalance may occur over time between the internal and external rotators, abductor and adductor muscles, and anterior and posterior shoulder muscles, which may further contribute to rotator cuff disorders [38].

Shoulder Force-Angle and Moment-Angle Relationships

Net joint forces and moments were higher when the shoulder was near its end range of motion on the push rim. As the speed of propulsion increased, the shoulder was in a compromised position as more significant relationships between the timing of the peak kinetics and maximum and minimum shoulder angles were found. Peak posterior force and sagittal extension moment consistently occurred before hand release when the shoulder was maximally flexed and minimally abducted. With increased speed, the magnitudes of this force and moment were greater and the timing between peak posterior force and the peak angles were closer together. With the arm in this position, the head of the humerus is potentially positioned more posteriorly and the added presence of a posteriorly directed force acts to drive the humerus rearward against the posterior capsule. This combination of shoulder position and peak loading condition may predispose the wheelchair user to shoulder injury. This is because greater depressive forces from the rotators and adductors are required to keep the head of the humerus from translating upward and compressing the soft tissues and tendons in the subacromial space. Wheelchair users in general exhibit posterior shoulder musculature weakness and a relative tightness in the anterior shoulder musculature [38]. Consequently, they are at a greater risk of injury when the shoulder is repetitively exposed to high loads and when the humerus is posteriorly oriented.

Shoulder abnormalities about the coracoacromial arch have been reported in wheelchair users with or without pain [6,39]. Medical evidence has confirmed that impingement of the rotator cuff supraspinatus muscle occurs against the anterior edge and undersurface of the anterior third of the acromion, the coracoacromial ligament, and at times the acromioclavicular joint [40]. All these structures lie anterior to the acromion, and with internal rotation, they become even more anterior. Combined with arm abduction, the supraspinatus muscle insertion passes under the coracoacromial ligament or the anterior process of the acromion, placing it in the most prone position for impingement [41]. Although not significant, sagittal flexion moment tended to peak near maximum shoulder abduction (**Figure 6**). For some individuals, their inferior forces and internal rotation angles were also quite large when the shoulder was most abducted. The abducted and internally rotated shoulder in conjunction with the repetitive and large axially directed forces along the humerus during propulsion may predispose wheelchair users to developing rotator cuff impingement syndrome.

An abnormal scapulothoracic motion is often observed among people with glenohumeral instability or impingement [42–45]. Paralysis that affects the dynamic stabilizers of the thoracoscapular joint (serratus anterior, trapezius, and rhomboid muscles) will further impact the ability of the glenohumeral joint to remain in congruent contact with the glenoid cavity when weight-bearing forces are present. The model that we used to investigate shoulder biomechanics during wheelchair propulsion provided only the net muscle forces and moments acting at the glenohumeral joint. A more detailed model that includes the dynamic interplay between the shoulder bones (scapula, clavicle, and humerus) and scapulothoracic gliding is needed for one to determine the simultaneous agonistic and antagonistic muscle forces and moments necessary for maintaining stability of the shoulder during wheelchair propulsion. In addition, our model neglects any translations of the humerus and only considers humeral rotations. The extent that the humerus translates within the joint may be a critical etiological factor in the development of shoulder abnormalities among wheelchair users.

CONCLUSIONS

This study provides a comprehensive description of the 3D net forces and moments acting at the shoulder and subsequent positioning of the shoulder during submaximal wheelchair propulsion. A clearer understanding of shoulder positioning and the loads acting at the shoulder during propulsion may reveal new therapies and interventions that minimize the risk of shoulder injuries. Close inspection of the data revealed that individuals differed from each other in terms of their shoulder range of motion, peak kinetics, and at what point during their stroke the peaks occurred. Future studies are needed to determine the association between relative timing of the peak shoulder kinetics and shoulder angles and the presence or absence of abnormal scapular kinematics, shoulder instability, and shoulder pathology. Longitudinal studies are also needed for one to determine if the shoulder variables used in this study are able to predict who is at risk for developing shoulder pain and injury. Moreover, it is important to determine alterations in shoulder kinetics and kinematics because of wheelchair configuration

and design features, stroke technique, positioning, and anthropometry. This information would help clinicians and consumers select wheelchairs and postures that promote efficient and safe propulsion.

REFERENCES

1. Curtis KA, Tyner TM, Zachary L, Lentell G, Brink D, Didyk T, Gean K, Hall J, Hooper M, Klos J, Lesina S, Pacillas B. Effect of a standard exercise protocol on shoulder pain in long-term wheelchair users. Spinal Cord 1999;37:421–29.
2. Pentland WE, Twomey LT. The weight-bearing upper extremity in women with long term paraplegia. Paraplegia 1991;29:521–30.
3. Gellman H, Sie I, Waters RL. Late complications of the weight-bearing upper extremity in the paraplegic patient. Clin Orthop 1988;233:132–35.
4. Nichols PJ, Norman PA, Ennis JR. Wheelchair user's shoulder? Shoulder pain in patients with spinal cord lesions. Scand J Rehabil Med 1979;11(1):29–32.
5. Sie IH, Waters RL, Adkins RH, Gellman H. Upper extremity pain in the postrehabilitation spinal cord injured patient. Arch Phys Med Rehabil 1992;73:44–48.
6. Lal S. Premature degenerative shoulder changes in spinal cord injury patients. Spinal Cord 1998;36(3):186–89.
7. Bednarczyk JH. Kinematics of wheelchair propulsion in adults and children with spinal cord injury. Arch Phys Med Rehabil 1994;75(12);1327:1334.
8. Rodgers MM, Gayle GW, Figoni SF, Kobayashi M, Lieh J, Glaser RM. Biomechanics of wheelchair propulsion during fatigue. Arch Phys Med Rehabil 1994;75:85–93.
9. Ridgway MP. A kinematic analysis of 800-meter wheelchair-racing techniques. Adapted Phys Act Q 1988;5(2): 96–107.
10. Rao SS, Bontrager EL, Gronley JK, Newsam CJ, Perry J. Three-dimensional kinematics of wheelchair propulsion. IEEE Trans Rehabil Eng 1996;4(3):152–60.
11. Davis LA, Growney ES. Three-dimensional kinematics of the shoulder complex during wheelchair propulsion: A technical report. J Rehabil Res Dev 1998;35(1):61–72.
12. Boninger ML, Cooper RA, Shimada SD, Rudy TE. Shoulder and elbow motion during two speeds of wheelchair propulsion: a description using a local coordinate system. Spinal Cord 1998;36:418–26.
13. Wang YT, Deutsch H, Morse M, Hedrick B, Millikan T. Three-dimensional kinematics of wheelchair propulsion across racing speeds. Adapted Phys Act Q 1995;12:78–89.
14. Newsam CJ, Rao SS, Mulroy SJ, Gronley JK, Bontager EL, Perry J. Three dimensional upper extremity motion during manual wheelchair propulsion in men with different levels of spinal cord injury. Gait Posture 1999;10(3):223–32.
15. van der Helm FC, Veeger HE. Quasi-static analysis of muscle forces in the shoulder mechanism during wheelchair propulsion. J Biomech 1996;29(1):39–52.
16. Veeger HEJ, van der Woude LH, Rozendal RH. Load on the upper extremity in manual wheelchair propulsion. J Hand Surg [Am] 1991;4(4):270–80.
17. Kulig K, Rao SS, Mulroy SJ, Newsam CJ, Gronley JK, Bontrager EL, Perry J. Shoulder joint kinetics during the push phase of wheelchair propulsion. Clin Orthop 1998; 354:132–43.
18. VanSickle DP, Cooper RA, Robertson RN. SMART^{Wheel}: Development of a digital force and moment sensing pushrim. Proceedings of the 18th Annual RESNA Conference; 1995 Jun 9–14; Vancouver, Canada. p. 352–54.
19. Cooper RA, Robertson RN, VanSickle DP, Boninger ML, Shimada SD. Methods for determining three-dimensional wheelchair pushrim forces and moments: a technical note. J Rehabil Res Dev 1997;34(2):162–70.
20. DiGiovine CP, Cooper RA, Boninger ML. Dynamic calibration of a wheelchair dynamometer. J Rehabil Res Dev 2001;38(1):41–55.
21. Cooper RA, Boninger ML, Shimada SD, Lawrence BM. Glenohumeral joint kinematics and kinetics for three coordinate system representations during wheelchair propulsion. Am J Phys Med Rehabil 1999;78(5):435–46.
22. Hanavan EP. A mathematical model of the human body. AMRL-TR-64-102. Wright-Patterson Air Force Base, Yellow Springs (OH); 1964.
23. Clauser CE, McConville JT, Young JW. Weight, volume and center of mass of segments of the human body. AMRL-TR-69-70. Wright-Patterson Air Force Base, Yellow Springs (OH); 1969.
24. Sanderson DJ, Sommer HJ. Kinematic features of wheelchair propulsion. J Biomech 1985;18:423–29.
25. van der Woude LHV, Veeger HEJ, Rozendal RH. Ergonomics of wheelchair design: A prerequisite of optimum wheeling conditions. Adapted Phys Act Q 1989;6:109–32.
26. Cicchetti DV, Aivano SL, Vitale J. A computer program for assessing the reliability and systematic bias of individual measurements. Educ Psychol Measurement 1976;(36): 761–64.
27. Cicchetti DV, Sparrow SA. Developing criteria for establishing interrater reliability of specific items: applications to assessment of adaptive behavior. Am J Ment Defic 1981;86(2):127–37.
28. Pearl ML, Harris SL, Lippitt SB, Sidles JA, Harryman DT, Matsen FA. A system for describing positions of the humerus relative to the thorax and its use in the presentation of several functionally important arm positions. J Shoulder Elbow Surg 1992;1:113–18.

29. Masse LC, Lamontagne M, O'Riain MD. Biomechanical analysis of wheelchair propulsion for various seating positions. J Rehabil Res Dev 1992;29(3):12–28.
30. Boninger ML, Baldwin MA, Cooper RA, Koontz AM, Chan L. Manual wheelchair pushrim biomechanics and axle position. Arch Phys Med Rehabil 2000;81:608–13.
31. van der Woude LHV, Veeger DJ, Rozendal RH, Sargeant TJ. Seat height in handrim wheelchair propulsion. J Rehabil Res Dev 1989;26(4):31–50.
32. Brubaker CE. Wheelchair prescription: An analysis of factors that affect mobility and performance. J Rehabil Res Dev 1986;23:19–26.
33. Bednarczyk JH, Sanderson DJ. Kinematics of wheelchair propulsion in adults and children with spinal cord injury. Arch Phys Med Rehabil 1994;75:1327–34.
34. Vanlandewijck YC, Spaepen AJ, Lysens RJ. Wheelchair propulsion: functional ability dependent factors in wheelchair basketball players. Scand J Rehabil Med 1994; 26(1):37–48.
35. Cooper RA. Rehabilitation Engineering: Applied to Mobility and Manipulation. Bristol (UK) and Philadelphia (PA): Institute of Physics Publishing; 1995.
36. Koontz AM, Boninger ML, Towers J, Cooper RA, Baldwin MA. Propulsion forces and MRI evidence of shoulder impairment. Proceedings of the American Society of Biomechanics 23rd Annual Meeting; 1999 Oct 21–23; Pittsburgh (PA). p. 296–97.
37. Veeger HEJ, van der Woude LHV, Rozendal RH. Load on the upper extremity in manual wheelchair propulsion. J Electromyogr Kinesiol 1991;1(4):270–80.
38. Burnham RS, May L, Nelson E, Steadward R, Reid DC. Shoulder pain in wheelchair athletes. The role of muscle imbalance. Am J Sports Med 1993;21:238–42.
39. Boninger ML, Towers JD, Cooper RA, Dicianno BE, Munin MC. Shoulder imaging abnormalities in individuals with paraplegia. J Rehabil Res Dev 2001;38(4):401–8.
40. Neer CS, II. Impingement lesions. Clin Orthop 1983;173: 70–77.
41. Neer CS, II. Anterior acromioplasty for the chronic impingement syndrome in the shoulder: A preliminary report. J Bone Joint Surg [Am] 1972;54:41–50.
42. Belling Sorensen AK, Jorgensen U. Secondary impingement in the shoulder. Scand J Rehabil Med Sci Sports 2000;10:266–78.
43. Ludewig PM, Cook TM. Alterations in shoulder kinematics and associated muscle activity in people with symptoms of shoulder impingement. Phys Ther 2000;80(3): 276–91.
44. Lukasiewicz AC, McClure P, Michener L, Pratt N, Sennett B. Comparison of 3-dimensional scapular position and orientation between subjects with and without shoulder impingement. J Orthop Sports Phys Ther 1999; 29(10):574–83.
45. Endo K, Ikata T, Katoh S, Takeda Y. Radiographic assessment of scapular rotational tilt in chronic shoulder impingement syndrome. J Orthop Sci 2001;6(1):3–10.

Submitted for publication January 10, 2002. Accepted in revised form June 17, 2002.